P1.7 **THE RELATION BETWEEN THE RADAR TO LIDAR RATIO AND THE EFFECTIVE RADIUS OF DROPLETS IN WATER CLOUDS: AN ANALYSIS OF STATISTICAL MODELS AND OBSERVED DROP SIZE DISTRIBUTIONS**

Oleg A. Krasnov * and Herman W. J. Russchenberg
International Research Centre for Telecommunications-transmission and Radar,
Faculty of Information Technology and Systems, Delft University of Technology, The Netherlands

1. INTRODUCTION

The size distribution of drops in water clouds plays an important role in the development of precipitation and interaction of solar radiation with clouds. The parameterizations of such impact using drop size distribution (DSD) itself usually are based on its representation with simple statistical models like monodisperse (d -function), gamma, log-normal, and uniform probability density functions. Such approach needs a priori information or assumptions about type of model distribution and its parameters. The presence of drizzle fraction makes applicability of the simple models of DSD questionable (Fox and Illingworth (1997), Krasnov and Russchenberg (2001)). On the other hand, most of applications are interested not in DSD itself but in some set of its moments. For example, Liou and Ou (1989) have shown that the amount of precipitation produced by cloud is proportional to the fourth power of cloud's drops mean radius. Slingo (1990) showed that a 2 - mm change of the effective radius of drops in stratocumulus could cause an effect on the radiation budget that is equal to a doubling of atmospheric CO_2. Another important fact is that measurable quantity in atmospheric remote sensing can be expressed via moments of DSD.

One of the most often-used parameter in cloud studies is the effective radius of cloud drops r_e (in some publications it is called median volume radius (diameter)) that is defined as the ratio between 3rd and 2nd moments of DSD. Recent studies (Baedi et al. (2000), Krasnov and Russchenberg, (2002)) have shown that it can be retrieved from simultaneous radar and lidar measurements using the relationship between r_e and the radar reflectivity Z to the lidar extinction a ratio.

This article reports some results of this relationship study and is organized as follows. In Section 2 we describe the observational in-situ data from a few different field campaigns that were used for analysis, and the methods of their processing. In Section 3 we derive the theoretical relationship between Z/a and r_e for a few statistical distributions. Then, in Section 4 we present observed in-situ data on the $Z/a - r_{eff}$ plane, discuss, fit and model the result relation. We show the possibility to use this plane for cloud type classification into three classes: the clouds without drizzle, the clouds with drizzle, and the drizzle clouds. Section 5 describes the application of the developed classification technique for the representation of observed data on the *LWC-Z* plane that allows to use different *LWC-Z* relationships for different cloud types. Finally, the Section 6 contains the conclusions.

* *Corresponding author address*: Oleg Krasnov, TU Delft, IRCTR, Mekelweg 4, 2628 CD, Delft, The Netherlands. e-mail: o.krasnov@irctr.tudelft.nl

2. EXPERIMENTAL DETAILS AND INSTRUMENTATION

2.1. Observational data used

2.1.1. The CLARE'98 campaign. The Cloud Lidar and Radar Experiment (CLARE) took place near Chilbolton (United Kingdom) in October 1998. This extensive cloud campaign included airborne and ground-based radar and lidar observations as well as in-situ aircraft measurements of the drop-size distributions (see ESA (1999) for details).

During CLARE'98 the particle size spectra in clouds were measured from a C-130 aircraft of the UK MRF with a Forward Scattering Spectrometer (FSS) and a Two-Dimensional Cloud (2DC) probes in the size ranges between 1 μm and 23.5 μm radius and between 6.25 μm and 406.25 μm radius, respectively. The available data have a 5-sec interval of averaging.

2.1.2. The DYCOMS-II campaign. The DYCOMS-II field campaign took place in July 2001 in Pacific Ocean near California (Stevens et al. (2002)). It was directed to collect data to study nocturnal marine stratocumulus. The main measuring part of campaign was made during 10 research flights of the NCAR's RAF EC-130Q. On this aircraft cloud droplet spectrums were measured using a set of probes: the PMS - PCASP 100; the PMS-FSSP-100; the PMS-FSSP-300; the PMS-260X; the PMS-2DC; and the PMS-2DP in the different size ranges between 0.045 and 786 μm radius. For in-situ measurements of LWC on aircraft two King hot-wire probes that were installed on different wings and the Gerber's Particulate Volume Monitor PVM-100A were used. The available data have a 1-sec interval of averaging.

2.1.3. The CAMEX-3 campaign. The third field campaign in the Convection And Moisture Experiment series (CAMEX - 3) took place in Florida coastal zone in August - September 1998. The objective of the field program was data collection for research in tropical cyclone using NASA-funded aircrafts ER-2 and DC-8, and ground-based remote sensing. For this study it was important that all research flights took place in strong cumulus clouds. For measurement of the cloud drop size distributions were used FSS (the size range between 0.42 μm and 23.67 μm radius) and 2DC (the size range between 17.75 and 762.50 μm radius) probes that were mounted on the DC-8. The available data have a 60-sec interval of averaging.

2.2. In-situ clouds particle spectrums data processing and analysis

The above presented descriptions of field campaigns and their instrumentation show that in

order to obtain a complete cloud DSD, the distributions that were measured by a few individual particle probes have to be merged. There are some possible techniques for such merging (e.g. Baedi et al. (1999)). For this study the simplest technique was used: all spectrum probes that had been taking into account for a given platform were analyzed on an equal basis. For every bin of every probe middle size was calculated, counted concentration was normalized by the bin's width. Then all bins for the probes were combined and rearranged in increasing order of their middle size values. The resulting grid of middle sizes was used for estimation of the values for new borders of bins - as half distance between neighbor bin's centers. Such approach gives the possibility to include in calculations all available data without any a priori assumptions about shape of DSD. Any moments of the resulting DSD can be calculated as numerical integrals for tabulated functions. Before the start of merging procedure from every probe's data first and last bins were removed as possible sources of error information (Francis (1999)).

Since this paper only deals with liquid water clouds, it was assumed that for radar observations the spherical drops act as Rayleigh scatterers, while for lidar observations they approximately act as optical scatterers. In that case, various cloud parameters can be computed from the particle size spectra using the following equations:

Radar reflectivity:

$$z = 64 \cdot \sum_i N_i \cdot r_i^6 \cdot \Delta r_i , \qquad [mm^6 \cdot m^{-3}] \qquad (1)$$

Lidar extinction cross-section:

$$a = 2 \cdot p \cdot \sum_i N_i \cdot r_i^2 \cdot \Delta r_i \cdot 10^{-6} , \; [m^{-1}] \qquad (2)$$

Liquid water content:

$$LWC = \frac{4 p r_w}{3} \cdot \sum_i N_i \cdot r_i^3 \cdot \Delta r_i \cdot 10^{-6} , [g \cdot m^{-3}] \qquad (3)$$

Effective radius:

$$r_e = \frac{\sum_i N_i \cdot r_i^3 \cdot \Delta r_i}{\sum_i N_i \cdot r_i^2 \cdot \Delta r_i} \cdot 10^3 , \; [mm] \qquad (4)$$

The ratio Z/a of radar reflectivity Z - to - lidar extinction a

$$\frac{Z}{a} = \frac{64}{2p} \cdot \frac{\sum_i N_i \cdot r_i^6 \cdot \Delta r_i}{\sum_i N_i \cdot r_i^2 \cdot \Delta r_i} \qquad (5)$$

where r_w is the density of water in $[kg \cdot m^{-3}]$, N_i is the normalized by bin width number of particles that were measured in i[th] bin $[m^{-3} \cdot mm^{-1}]$, r_i and Δr_i are the mid-radius and width of i[th] bin $[mm]$.

3. THE $Z/a - r_{eff}$ RELATIONSHIP FOR SIMPLE STATISTICAL MODELS OF DSD

Usually for the representation of the cloud DSD the standard statistical probability functions with similar shapes are used. In many publications the different modifications of gamma probability density functions were applied. Such representation of DSD can be written in form:

$$N(D) = \frac{N_0}{D_{m,gam}^n \cdot \Gamma(n)} \cdot D^{n-1} \cdot e^{-\frac{D}{D_{m,gam}}} , \; D \geq 0 , \qquad (6)$$

where $\Gamma(n)$ - the gamma function, n and $D_{m,\,gam}$ - shape and scale parameters of gamma distribution. Using equations for the moments of this distribution (e.g. Krasnov and Russchenberg (2001)), the relation between radar-to-lidar ratio and effective radius of drops can be expressed as:

$$\frac{Z}{a} = \frac{64}{2p} \cdot \left[\prod_{i=2}^{5} \left(1 + \frac{i}{n}\right) \right] \cdot {r_m}^4 = \frac{64}{2p} \cdot \frac{(n+3) \cdot (n+4) \cdot (n+5)}{(n+2)^3} \cdot r_{eff}^4 \qquad (7)$$

For $n = 1$ equations (6) and (7) describe the exponential DSD. For the other type of the model DSD – log-normal, that is also widely used in the publications for the representation of drops spectrum in water clouds:

$$N(D) = \frac{N_0}{D \cdot s_{\log} \cdot \sqrt{2 \cdot p}} \cdot e^{-\frac{\left[\ln(D / D_{m,log})\right]^2}{2 \cdot s_{\log}^2}} , \qquad (8)$$

$$D \geq 0$$

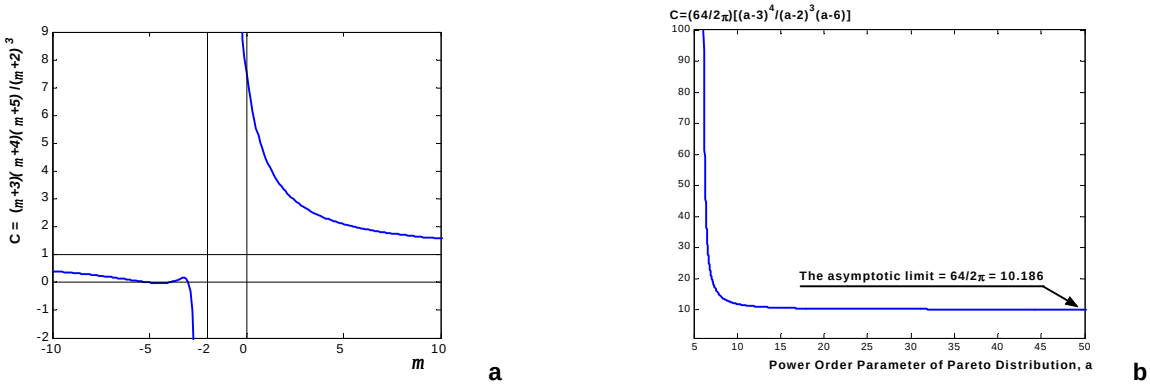

Fig.1. Factor C from relationship $Z/a = C \cdot r_{eff}^4$ as function of the shape parameters of distribution: (a) for the gamma drop size distributions, (b) for Pareto drop size distributions.

where $s_{\log}$ and $D_{m,\log}$ - shape and scale parameters of the log-normal distribution, the $Z/a - r_{eff}$ relationship can be written as:

$$\frac{Z}{a} = \frac{64}{2p}\cdot\exp\left(14\cdot s_{\log}^{2}\right)\cdot {r_m}^4 = \\ = \frac{64}{2p}\cdot\exp\left(6\cdot s_{\log}^{2}\right)\cdot r_{eff}^4 \quad (9)$$

When the shape of DSD, which is represented in $\log(N)$ - $\log(r)$ scales, is closed to the linear function, it is possible to use the Pareto model distribution (e.g. Johnson and Kotz (1970)):

$$p_X(x) = \frac{a\cdot k^a}{x^{a+1}}, \quad k>0,\, a>0,\, x\ge k. \quad (10)$$

Provided n is less then a, the n^{th} moment about zero is

$$m_n = \frac{a\cdot k^n}{a-n}. \quad (11)$$

Using (11) the effective radius of cloud droplets r_{eff} and the relationship between Z/a ratio and r_{eff} can be written:

$$r_{eff} = k\,\frac{a-2}{a-3}, \quad (12)$$

$$\frac{Z}{a} = \frac{64}{2p}\cdot\frac{(a-3)^4}{(a-2)^3\cdot(a-6)}\cdot r_{eff}^4, \; a>6 \quad (13)$$

From (7), (9) and (13) follows that for these model distributions exist the 4th power relationship between the ratio Z/a and the effective radius r_{eff}. The factor C in the equation $Z/a = C\cdot r_{eff}^4$ for every statistical distribution depends on one parameter that describes the shape of distribution. For the Pareto distribution this parameter is the power order a and it is necessary to note that this parameter has to satisfy the condition $a>6$, otherwise applicability of Pareto distribution model for DSD is questionable. For the log-normal distribution factor C increases with arising of shape parameter s monotonically. For the gamma distribution and for the Pareto distribution such dependencies are presented on Fig. 1. For the gamma distribution parameter C is positive for $n\in(-\infty,-5]\cup[-4,-3]\cup[-2,+\infty)$, has the point of discontinuity $m=-2$, and for $n\to\pm\infty$ has asymptotic value $C = 64/2p$. For the Pareto distribution this factor is dropped down very fast with arising of power order a. For $a>10$ its value is closed to $64/2p$ that is correspond with such value for the d-function like distribution.

4. OBSERVATIONAL RESULTS

4.1. Observed $Z/a - r_{eff}$ relation

The merged DSD data for above described field campaigns were used for calculation of Z/a ratio and r_{eff}. Then, following Baedi et al. (2000), these pairs of parameters were depicted as a scatter plot

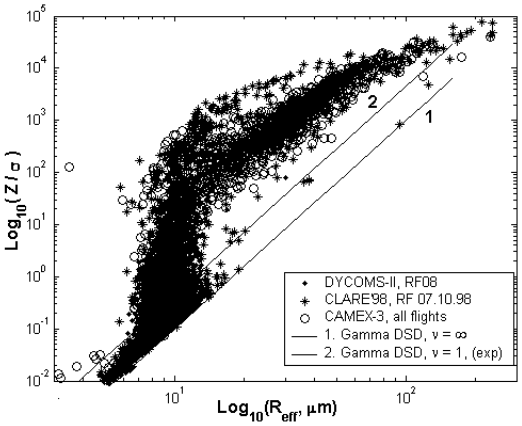

Fig. 2. The Radar to Lidar Ratio versus the Effective Radius for the CLARE'98, DYCOMS-II, and CAMEX - 3 campaigns data

with logarithmic scale. The resulting graph is presented on Fig. 2. On the same figure two theoretical relationships for gamma distributions with extreme values of their shape parameter n ($n=\infty$, that correspond to the narrow, d-function-like gamma distribution, and $n=1$, that correspond to the exponential distribution) also are presented.

First important conclusion that follows from this representation is that all data that were measured in different geographical regions, inside different types of water clouds, and during different field campaigns with different sets of the cloud's particle probes have the similar behavior. It means that observed dependence has stable character and can be used as background for the development of cloud microphysics retrieval algorithm.

The comparison of observed data with theoretical dependencies shows that the behavior of the $Z/a - r_{eff}$ relationship for observed data has a complicated difference with theoretical 4th power relationship. The $Z/a - r_{eff}$ plane can be divided into three clear visible areas:

I. The area with small values of the Z/a ratio and r_{eff}. In this area all observed data are placed between lines that represent the narrow, d-function-like distribution, and the exponential distribution. For this set of DSD standard fitting with simple statistical models (gamma and log-normal DSD) can be used;

II. The central area of the $Z/a - r_{eff}$ plane (r_{eff} around 10 mm) is characterized by fast arising of the Z/a ratio with small increasing of r_{eff};

III. The upper area of the $Z/a - r_{eff}$ plane is characterized by slow increasing of the Z/a ratio with arising of r_{eff} (about 2 time less then for model distributions), with asymptotic convergence to the area of model DSD with big r_{eff}.

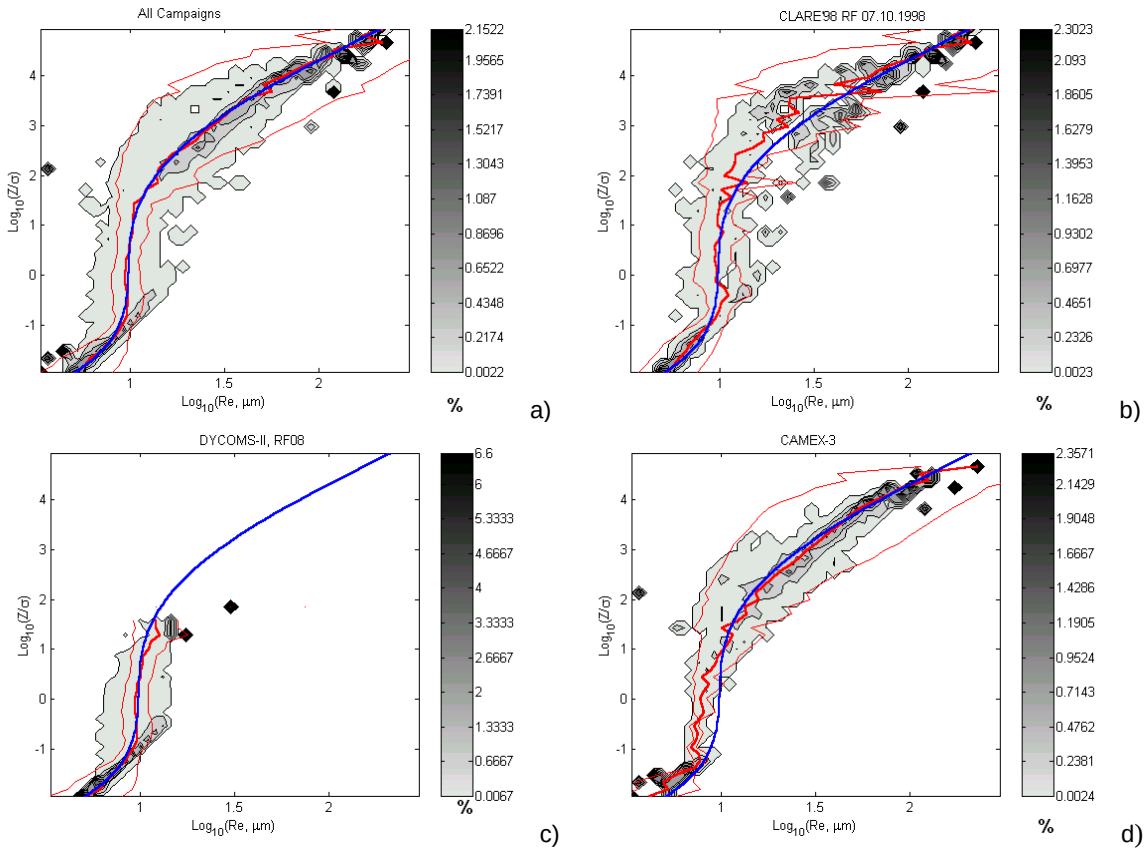

Fig. 3. Two-dimensional histograms for the observed $Z/a - r_{eff}$ relations with mean and standard deviations and their fitting using the 4th order polynomial (1): for all campaigns data (a), for the CLARE'98 RF 07.10.1998 data (b), for the DYCOMS-II RF08 data (c), and for the CAMEX-3 data (d).

The DSD, which are placed in the areas II and III of the $Z/a - r_{eff}$ plane, can not be described with simple statistical model distribution like gamma or log-normal, that have observable shape parameters. The n parameter of gamma DSD in these areas has to have negative values, for log-normal DSD s parameter has to have values more then unity. In both cases the resulting shape of model distribution is not compatible with the shape of observed DSD.

This result has good agreement with Baedi et al. (2000) and Krasnov and Russchenberg, (2001), where were shown that representation of the drop size distribution as gamma probability density function is possible only for distributions that have radar reflectivity less then some threshold level. For data that were measured during the CLARE'98 campaign this threshold level Z_0 estimated as -30 dB. For the CAMEX-3 data Z_0 = -60 dB, and for the DYCOMS-II campaign's research flight RF08 Z_0 = -25 dB. Difference between threshold values for the different campaigns can be explained with assumption of different nature of observed clouds. For the DYCOMS-II campaign's research flight RF08 there were stratiform clouds without drizzle mode, for the CLARE'98 there were stratiform clouds with drizzle, and for the CAMEX-3 there were convective clouds with prevalent drizzle mode.

4.2. Fitting of observed results

For the parameterization of observed during the CLARE'98 campaign $Z/a - r_{eff}$ dependence in Baedi et al. (2000) the piecewise-linear fitting of areas I-III was used:

$$\log_{10}\left(\frac{Z}{a}\right) = \begin{cases} -4.60 + 4.06 \cdot \log_{10}\left(r_{eff}\right), \\ \qquad\qquad Z < -35dB \\ -34.93 + 40.20 \cdot \log_{10}\left(r_{eff}\right), \\ \qquad\qquad \log_{10}\left(Z/a\right) < 1.7 \\ -0.49 + 2.40 \cdot \log_{10}\left(r_{eff}\right), \\ \qquad\qquad \log_{10}\left(Z/a\right) \geq 1.7 \end{cases} \quad (14)$$

For this study it was necessary to repeat fitting procedure because we used different methods for merging and calibration the CLARE'98 campaign's DSD and were added data from another campaigns. It was found that the results of such fitting are strongly depended on the method that had used for the division of the $Z/a - r_{eff}$ plane into the areas for regional linear fitting. For example, for the separation the area II from the area III (following described above classification) were used a few equations for the linear boundaries of areas and the followed estimations of the coefficients for the linear equation $\log_{10}\left(Z/a\right) = a \cdot \log_{10}\left(r_{eff}\right) + b$ were calculated: $a = 18 \ldots 71$ and $b = -18 \ldots -68$. These very big

variations of the results and absence of the theoretical basis for the $Z/a - r_{eff}$ plane division means that such piecewise-linear fitting is relatively voluntary.

As the alternative of such approach was made the try to estimate possibility to find high order polynomial fitting that is stable for all campaigns in whole area of interest on the plane $Z/a - r_{eff}$ ($-2 \le \log_{10}(Z/a) \le 5, \quad -0.5 \le \log_{10}(r_{eff}) \le 2.5$). Using MATLAB function for polynomial fitting, the reliable solution for the $r_{eff} = F(Z/a)$ dependency was found as a 4th order polynomial:

$$\begin{aligned}\log_{10}(r_{eff}) = &-0.0027\cdot(\log_{10}(Z/a))^4 + \\ &+0.026\cdot(\log_{10}(Z/a))^3 - \\ &-0.0094\cdot(\log_{10}(Z/a))^2 + \\ &+0.0098\cdot(\log_{10}(Z/a)) + 0.99\end{aligned} \qquad (15)$$

The point of curve inflection is $\log_{10}(Z/a) = 0.124$, $\log_{10}(r_{eff}) = 0.991$. For $\log_{10}(r_{eff}) > 1.1$ this curve can be fitted by linear function, that are practically equal to third equation in (14). For $\log_{10}(r_{eff}) < 0.95$ the same procedure gives the best linear fitting that was determined from observed data with $Z \le -35$ dB:

$$\log_{10}(Z/a) = 4.6363 + 3.842\cdot\log_{10} r_{eff} \qquad (16)$$

The equation (15) is presented on Fig. 3 where it is depicted with two-dimensional histograms of observed data for all campaigns together (Fig. 3a) and for every campaign separately (Fig. 3b, c, d). From these representations it can be seen that the estimated using joint two-dimensional histogram for all campaigns data equation (15) has reasonable good agreement with the CLARE'98 and the DYCOMS-II data for stratiform clouds. For cumulus clouds, which were observed during the CAMEX-3 campaign, the noticeable difference in the region of maximal variability of the Z/a ratio (area II) can be seen. For this campaign observed values of effective radius of cloud drops in this region for a given Z/a ratio are shifted to lowest values. This fact can be explain as natural difference of the stratiform and cumulus clouds – in cumulus clouds the drizzle fraction has to be taken into account for DSD that have smallest effective radiuses.

As result can be made the conclusion that the investigated by Baedi et al. (2000) behavior of the observed DSD on the $Z/a - r_{eff}$ plane is relatively stable. The variations in empirically estimated parameters for different geographical regions, field campaigns, and different types of cloud are reasonable small. For the description of this dependence can be used a 4th order polynomial or piecewise-linear relationships. For the area I and for the area III both approaches give the similar results. There are difference in the linear and nonlinear equations in the area II that is characterized by the big variability in the Z/a ratio – from –1.0 up to 1.5..2, but for both of these approaches this region is characterized by small variability of the effective radius of cloud drops – from 8.9 to 12.5 mm.

4.3. The result interpretation and discussion

The presented above results demonstrate that observed DSD in water clouds have complicated behavior on the $Z/a - r_{eff}$ plane, which can not be explained using simple statistical models. In Baedi et al. (2000) have proposed to use the model that represent DSD in water clouds as a mixture of the gamma and the exponential distributions:

$$N(r) = N_0\begin{bmatrix} p\cdot W_{gam}(n, D_{m,gam}, r) + \\ +(1-p)\cdot W_{\exp}(D_{m,\exp}, r)\end{bmatrix} \qquad (17)$$

where $p = N_{gam}/N_0$ is the ratio of drop's concentration in gamma distributed fraction to the total concentration $N_0 = N_{gam} + N_{\exp}$ of cloud drops. Such model has good agreement with observed merged spectra, which show much slow decreasing of concentration in big particles area then it can be described with gamma or log-normal DSD.

The shape of the tail area of merged measured distribution, when it is presented in $\log(N) - \log(r)$ scales is closed to the linear function. For such reason it is possible to use for representation of this tail area of DSD (and as second term in mixture (17)) the Pareto distribution (10).

The utilization of such models for the representation of cloud DSD is useful, among other reasons, from the viewpoint of microphysical interpretation of the observed drop-size spectra. The first term in mixture (17) represents cloud droplets, and the second - drizzle fraction. The knowledge of p gives the possibility to classify cloud type into two (or more) classes - the cloud without drizzle and the cloud with drizzle fraction. And from this point of view the observed $Z/a - r_{eff}$ relationship is very promising.

4.3.1. The mixture's moments calculation. The detailed notation of (17) for both analyzed models of the mixed distributions is complicated and we did not

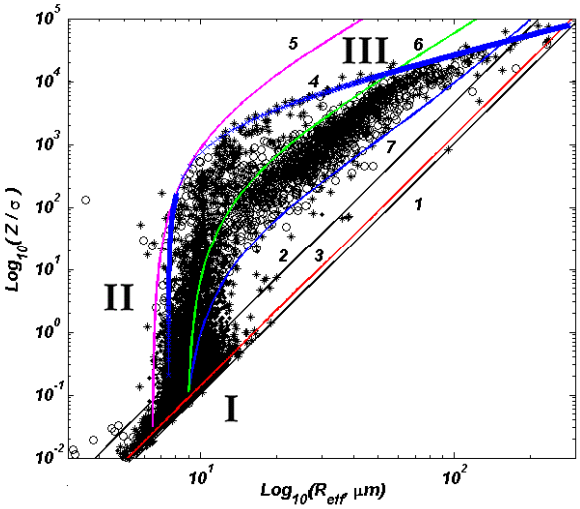

Fig. 4. Comparison of the behavior of observed data, simple statistical models, and mixtures of model distribution on the $Z/a - r_{eff}$ plane (see notation in text)

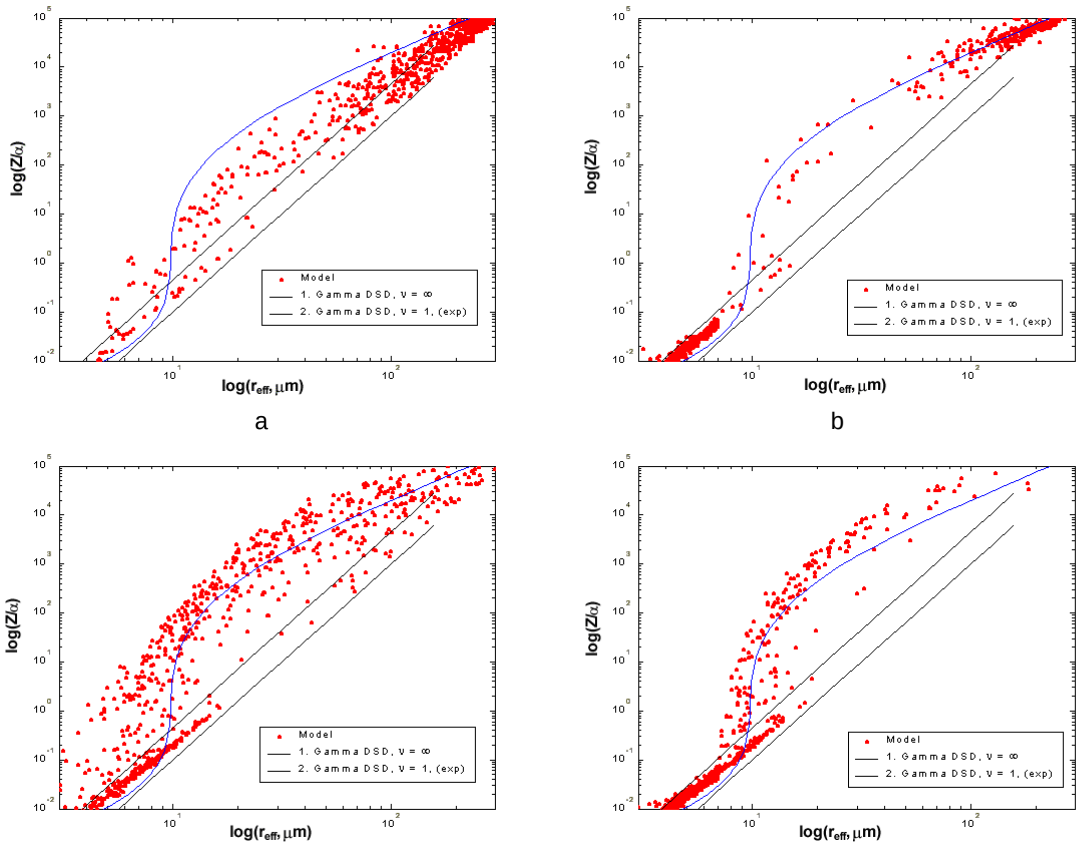

Fig.5. The results of Monte-Carlo modeling of the mixture of the gamma and the exponential DSD.

(a) $p = N_{\exp} / N_{gam} < 10^{-2}$, $R_{thres} = 0$; (b) $p = N_{\exp} / N_{gam} < 10^{-2}$, $R_{thres} = 7\ mm$;

(c) $p = N_{\exp} / N_{gam} < 10^{-4}$, $R_{thres} = 0$; (d) $p = N_{\exp} / N_{gam} < 10^{-4}$, $R_{thres} = 7\ mm$.

find analytical equation for the $Z/a - r_{eff}$ relationship. We used numerical methods for the calculations of the moments. On Fig.4 some results of such calculations in combination with observed data are presented. The numbered lines on this figure represent the model distributions. The line 1 represent the d -function-like DSD, line 2 - the exponential DSD, and line 3 - the uniform DSD. The line 4 represent the $Z/a - r_{eff}$ relationship for the mixture of the gamma DSD ($D_{m,gam} = 0.75$, $n = 8$, $r_{eff,gamma} = 7.5\ mm$) and the Pareto DSD ($a = 10$, $k = 250\ mm$, $r_{eff,Pareto} = 286\ mm$). Parameter $p_P = N_{paretto} / N_{gamma}$ during calculation changed between 0 and 0.1, but for calculation in the area II of the $Z/a - r_{eff}$ plane it was necessary to decrease upper limit. In area II parameter p_P was changed between 0 and 10^{-6}. Lines 5 - 7 represent the mixtures of the gamma DSD($n = 8$) and the exponential DSD during changes of scale parameter $D_{\exp}$ of exponential distribution between 1 and 200 mm for a few combinations of other parameters: for line 5 $D_{gam} = 0.65$, $N_{\exp}/N_{gam} = 10^{-4}$; for line 6 $D_{gam} = 0.90$, $N_{\exp}/N_{gam} = 0.003$; and for line 7 $D_{gam} = 0.90$, $N_{\exp}/N_{gam} = 0.05$.

From this representation follows that the behavior of observed spectrums in the area II of the $Z/a - r_{eff}$ plane can be explained using mixtures of distributions, which have very small ratio of the drizzle fraction concentration to the droplet concentration. For this area the portion of drizzle particle influences on radar reflectivity (and radar to lidar ratio) but still is not big enough to influence the effective radius. In the area III the drizzle fraction increases its influence on effective radius and, as result, in the upper part of the $Z/a - r_{eff}$ plane the simple statistical distributions can completely describe the behavior of observed DSD.

4.3.2. The Monte-Carlo simulation. Another possibility to analyze $Z/a - r_{eff}$ dependence for mixture of model distribution is the Monte-Carlo simulation. We used this method for the mixture of gamma and exponential distributions. Below we give the detail description of the model.

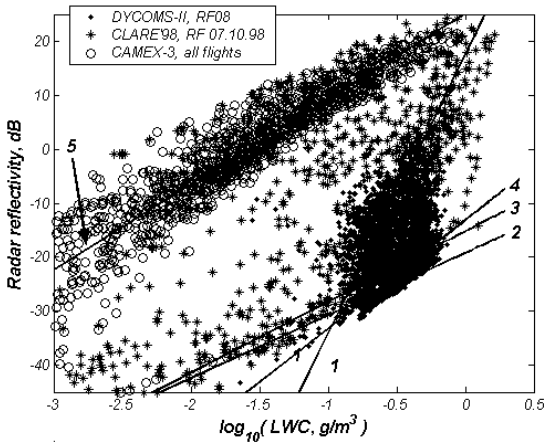

Fig.6. The relation between measured Liquid Water Content and Radar Reflectivity for different field campaigns. Lines represent the different linear fittings of this relation (see text for notation).

For every realization of gamma DSD the parameters N_{gam}, $D_{m,\,gam}$, and n were selected as random variables with the normal probability density function. For N_{gam} the mean value m_{N_0} = 74 cm^{-3} and the standard deviation s_{N_0} = 45 cm^{-3} from Miles et al. (2000) for marine stratocumulus was used, for $D_{m,\,gam}$ were used mean value $m_{\mathrm{D_{m,\,gam}}} = 1.1$ and standard deviation $s_{\mathrm{D_{m,\,gam}}} = 0.2$, for n - $m_n = 3.0$ and $s_n = 3.0$. For the estimation of the number of counted particles (model of in-situ probe) the sample cross-section of FSSP S = 0.2 mm^2 (Baedi (1999)) in following algorithm was used. At first, the random value of concentration with unit 1/cm^3 N_{gam} was generated as normal random variable with parameters m_{N_0} and s_{N_0}. Then, using relation between concentration N_{gam} and number of counted particles N_{cp}: $N_{cp} = N_{gam} \cdot S \cdot L$, where L is the length of sample measurement in cloud (typically for FSSP $L = 100$ m for 1 s sampling ratio and 1 km for 10 s sampling ratio), the number of counted particles was calculated as $N_{cp} = 200 \cdot N_{gam}$. Independent random generators were used for generation of the values for $D_{m,\,gam}$ and n. All these values were used as input of gamma random generator, which generated N_{cp} random numbers with gamma probability density function.

For the drizzle fraction was used exponential model of drop size distribution:

$$N(D) = \frac{N_{\exp}}{D_{m,\exp}} e^{-\frac{D}{D_{m,\exp}}} \qquad (18)$$

The concentration $N_{\exp}$ was derived from concentration of gamma DSD for small particles as $N_{\exp} = p \cdot N_{gam}$, where for factor p was used uniform probability distribution with specified minimal and maximal values. The scale parameter $D_{m,\exp}$ was generated as independent random variable that is uniformly distributed in interval [1,500] mm. For the calculations were not used the drops with sizes more than 400 mm.

During modeling it was possible two test two alternative hypothesis: (1) the drizzle is presented in every cloud, and (2) the drizzle is presented only in cloud with effective radius that is bigger than some threshold value R_{thres}. This parameter was included into the model. For nonzero R_{thres} drizzle fraction (exponential distribution) was added in result distribution only if the effective radius of gamma distribution was more than R_{thres}.

On Fig.5 a few resulting scattering plots, which were modelled for two upper values of the proportion between exponential and gamma concentration (10^{-2} and 10^{-4}) and for two values of threshold parameter R_{thres} (0 and 7 mm), are presented. From these plots it possible to see importance of the ratio between concentration of drizzle fraction and cloud droplets. The modeling results show reasonable agreement with observed data only for very small values of proportion $p = N_{\exp} / N_{gam}$, which are less then 10^{-4}. The comparison of the modeling results with observed data shows also importance of the parameter R_{thres} - when it is equal to zero, we have much wide scattering of resulting points that is not exist in observed dependence. As result the conclusion that drizzle fraction can exist only in clouds, which have effective radius more then some threshold value, can be made.

The presented above analysis and discussion show that complicated behavior of the observed data on the $Z/a - r_{eff}$ plane is caused by influence of drizzle fraction. It is possible to use it for simple classification of cloud's type with the criterion of presence and amount of drizzle fraction. The area I on the $Z/a - r_{eff}$ plane describes the cloud without drizzle. For such clouds simple statistical modes like gamma or log-normal DSD are applicable. The area III describes the clouds with strong drizzle fraction. We note such clouds as the drizzle clouds. And area II describes the transition area - the drizzle mode already exists, but its concentration is very small, and it influences only radar reflectivity. Such clouds we note as the clouds with drizzle.

5. APPLICATION FOR THE PARAMETERIZATION OF THE $Z - LWC$ RELATIONSHIP

Consider now the application of described above results for the parameterization of the $Z - LWC$ relation in water clouds. On Fig.6 are presented in-situ data for all three campaigns on the $Z - LWC$ plane. On the same figure are presented a few known approximations for this relationship:

1. (Baedi et al., 2000):

$$\log_{10}\left(Z_{merged}\right) = \\ = 1.76 + 5.17 \cdot \log_{10}\left(LWC_{merged}\right) \qquad (19)$$

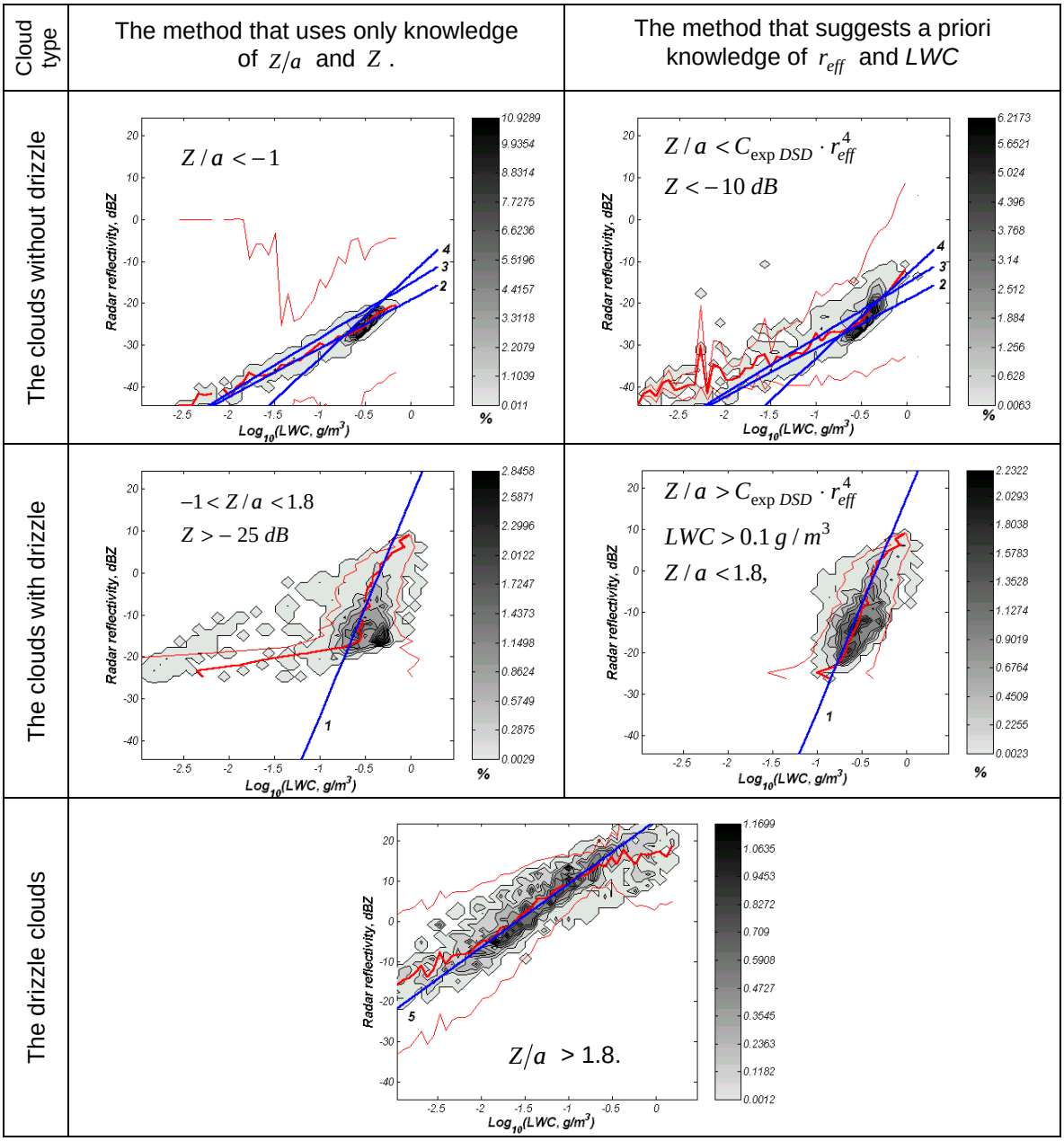

Fig. 7. Two-dimensional histograms for the $Z-LWC$ relation (with mean, standard deviations, and linear fittings) for different criteria and methods of cloud's type classification

2. (Fox and Illingworth, 1997):

$$\log_{10}(Z_{merged}) = \\ = \log_{10}(0.012) + 1.16 \cdot \log_{10}(LWC_{merged}) \quad (20)$$

3. (Sauvageot and Omar, 1987):

$$\log_{10}(Z_{merged}) = \\ = \log_{10}(0.03) + 1.31 \cdot \log_{10}(LWC_{merged}) \quad (21)$$

4. (Atlas, 1954):

$$\log_{10}(Z_{merged}) = \\ = \log_{10}(0.048) + 2.00 \cdot \log_{10}(LWC_{merged}) \quad (22)$$

5. Best fit of all data for the CAMEX-3 campaign and the CLARE'98's data for the drizzle clouds:

$$\log_{10}(Z_{merged}) = \\ = 2.51 + 1.58 \cdot \log_{10}(LWC_{merged}) \quad (23)$$

It can be seen from Fig. 6 that (20) - (22) describe only the clouds without drizzle, (19) can be applied for the clouds with drizzle, and (23) - for the drizzle clouds. The precision of these approximations is not discussed here – the dependencies are clearly visible and can be fitted using different methods. The main problem that follows from the Fig. 6 is how to separate these cloud types with remote sensing equipment for selection of the specific dependency (19)-(23) for every observed Z. The possibility to use the $Z/a - r_{eff}$ relation for classification of water cloud can be seen from Fig. 7. On this figure two-dimensional distributions of in-situ observed DSD that

are placed on the $Z-LWC$ plane after their classification are presented. For such classification two methods were used. The first method requires the knowledge about in-situ measured parameters - r_{eff} and *LWC*. The second method is based only on the results of radar and lidar measurements of Z/a and Z. The criteria for classification of the cloud type and selection of the $Z-LWC$ relationship also are presented on the Fig. 7.

On the same figures linear approximations, applicable for specific situations, are placed, and it can be seen that for such methods of the clusterization the known linear approximations of the $Z-LWC$ relation are not far from reality.

From the Fig. 7 follows the conclusion about the possibility to use the Z/a ratio for clusterization of $Z-LWC$ plane into sub-regions that describe clouds with different nature and can be parameterized by different equations. Such method can be used for cloud classification and improvement of cloud microphysics retrieval technique.

6. CONCLUSIONS

The presence of stable $Z/a - r_{eff}$ relationship for the different geographical locations, different field campaigns and different cloud types was demonstrated. It is possible to use for all analyzed campaigns and cloud types a unified 4th order polynomial fitting of this relationship. The complicated character of observed $Z/a - r_{eff}$ dependence in water clouds is caused by the influence of drizzle fraction. The analysis and statistical modeling demonstrated that it is possible to use the position of drop-size spectrum on the $Z/a - r_{eff}$ plane for the detection of drizzle fraction and to classify with such criterion clouds into three classes - the cloud without drizzle, the cloud with drizzle, and the drizzle cloud.

The algorithm for the classification of drop size distribution and cloud's type using measured radar to lidar ratio for the clusterization in the $Z-LWC$ plane were applied. It was shown that for every resulting cluster of cloud's type is possible to use specified type of the linear $Z-LWC$ relation.

The results can be used for the quality improvement of the retrieval algorithms of microphysical cloud parameters that use data from ground-based or space-based remote sensing instruments, like radar and lidar.

Acknowledgments. The data used in this paper were collected during the CLARE'98 campaign carried out under the auspices of the European Space Agency (ESA, (1999)). The FSSP and 2-DCP data sets for this campaign were kindly provided by P.Francis from the U.K. Met. Office. The airborne measurements obtained from the NSF/NCAR RAF EC-130Q aircraft during the DYCOMS-II project are available online from http://www.joss.ucar.edu/dycoms/. The access to this site was kindly provided by Bjorn Stevens. The CAMEX-3 DC-8 FSSP and 2-DC data provided by the GHRC at the Global Hydrology and Climate Center, Huntsville, Alabama. Our research received funding from the Netherlands Space Agency (SRON) under project EO - 035.

REFERENCES

Atlas, D., 1954: The estimation of cloud content by radar. *J. Meteor*., 11, 309-317.

Baedi, R.J.P., J.J.M. de Wit, H.W.J. Russchenberg, J.P.V. Poiares Baptista, 1999: Alternative algorithm for correcting FSSP measurements, *Proc. Int. workshop CLARE'98*, ESA-ESTEC, 123-127.

Baedi, R.J.P., J.J.M. de Wit, H.W.J. Russchenberg, J.S. Erkelens and J.P.V. Poiares Baptista, 2000: Estimating Effective Radius and Liquid Water Content from Radar and Lidar Based on the CLARE'98 Data-Set. *Phys. Chem. Earth (B)*, 25(10-12), 1057-1062.

ESA, 1999: CLARE'98: Cloud Lidar And Radar Experiment, International Workshop Proceedings. WPP - 170, ISSN 1022-6556, ESTEC, Noordwijk, The Netherlands, 239 pp.

Fox, N.I. and A.J. Illingworth, 1997: The retrieval of stratocumulus cloud properties by ground-based cloud radar. *J. Appl. Meteor*., 36, 485-492.

Francis, P.N., 1999: An Overview of the UKMO C-130 Measurements from CLARE'98*, Proc. Int. workshop CLARE'98, ESA-ESTEC*, 43-46.

Johnson, N.L., and S. Kotz, 1970: *Distributions in Statistics. Continuous Univariate Distributions-1*. Houghton Mifflin Company, Boston. - 300 pp.

Klett, J.D., 1983: Stable analytical inversion solution for processing lidar returns. *Appl. Opt.*, 20, 211-220.

Krasnov, O. A., and H.W.J. Russchenberg, 2001:Comparison of analytical approximations of the shapes of the cloud dropsize distributions, utilized for the interpretation of remote sensing data. *Preprints, 30th Conference on Radar Meteorology*, Munich, Germany, American Meteorological Society, Boston, pp. 559-561.

Krasnov, O.A., and H.W.J. Russchenberg, 2002: The Comparative Study of the Relation between Cloud Microphysics and Radar-to-Lidar Ratio for the Different Geographical Regions and Field Campaigns. *Proc. of Open Symposium on Propagation and Remote Sensing URSI Commission-F, Garmisch-Partenkirchen, Germany, 12th to 15th February 2002 (on CD-ROM)*, 10 pp.

Liou, K.N., and S.C. Ou, 1989: The role of cloud microphysical processes in climate: An assessment from a one-dimensional perspective. J. Geophys. Res., **94**, 8599-8607

Slingo, A., 1990: Sensitivity of the Earth's Radiation Budget to Changes in Low Clouds Nature. **343**, p. 49-51.

Sauvegeot, H. and J. Omar, 1987: Radar reflectivity of cumulus clouds. *J. Atmos. Oceanic Technol.*, **4**, 264-272.

Stevens, B., D.H. Lenschow, G. Vali, et al, 2002: Dynamics and Chemistry of Marine Stratocumulus – DYCOMS-II. *Bulletin of the American Meteorological Society*, in press.